Effects of anisotropy and magnetic fields on two-electron parabolic quantum dots

2004 J. Phys.: Condens. Matter 16 3633

(http://iopscience.iop.org/0953-8984/16/21/012)

INSTITUTE OF PHYSICS PUBLISHING JOURNAL OF PHYSICS: CONDENSED MATTER

J. Phys.: Condens. Matter **16** (2004) 3633–3646 PII: S0953-8984(04)78118-7

Effects of anisotropy and magnetic fields on two-electron parabolic quantum dots

P S Drouvelis[1], P Schmelcher[1,2] and F K Diakonos[3]

[1] Theoretische Chemie, Universität Heidelberg, Im Neuenheimer Feld 229, D-69120 Heidelberg, Germany
[2] Physikalisches Institut, Philosophenweg 12, Universität Heidelberg, D-69120 Heidelberg, Germany
[3] Department of Physics, University of Athens, GR-15771 Athens, Greece

E-mail: panos@tc.pci.uni-heidelberg.de (P S Drouvelis), peter@tc.pci.uni-heidelberg.de (P Schmelcher) and fdiakono@cc.uoa.gr

Received 19 March 2004
Published 14 May 2004
Online at stacks.iop.org/JPhysCM/16/3633
DOI: 10.1088/0953-8984/16/21/012

Abstract

An investigation of the combined effects due to the electronic interaction, anisotropy and the magnetic field interaction for two-electron quantum dots with harmonic confinement is performed. The electronic level structure and the dynamics of the dot are studied with varying field strength and anisotropy. The magnetization is derived for the complete deformation regime covering the regime of weak to strong fields. The cases without and with inclusion of the spin Zeeman interaction for a GaAs semiconductor are considered. The classical dynamics of the interacting electrons is studied and exhibits near integrability for field strengths leading to ratios $\omega_1{:}\omega_2 = 1{:}n$.

(Some figures in this article are in colour only in the electronic version)

1. Introduction

Quantum dots (QDs) allow one to confine electrons completely in a spatial region of several nanometres. Their main advantage is the high degree of control of the underlying experimental conditions such as the number of confined electrons and the shape of the artificial effective confinement. A wealth of literature devoted to these systems has exhibited their low dimensional atomic-like characteristics both theoretically [1] and experimentally [2]. Most of the investigations so far have assumed a circularly symmetric harmonic confinement due to the fact that the pronounced shell structure measured in the addition energy spectra of QDs is a direct consequence of it [3]. One of the most powerful tools for studying the electronic properties of few-electron quantum dots, in a 'clean' and accurate way, is the configuration

interaction method which has been employed extensively [4–26]. Additionally, the few-electron problem allows one to apply various other theoretical approaches such as perturbative techniques [27–30], semiclassical analysis [31–33] and Padé approximation [34].

Imposing external magnetic fields leads to a variety of new and unexpected properties. The ground state parity oscillations [35, 36] and the magic numbers in the angular momentum [4, 7, 37–40] are beautiful manifestations of the response of the interelectronic interaction to the magnetic field. Experimentally, the magnetic field has been a useful tool for probing the electronic structure of QDs. Hence, the change of the parity in the ground state was identified as a kink in the addition energy spectra [41–45] and the excitation spectrum of a QD could be probed and compared with exact calculations [2, 46]. Moreover, the response of the many-electron QD to magnetic fields has revealed further rich scenarios. For the low field regime, the measurements were explained within the constant-interaction model taking into account the exchange interaction between electrons with parallel spins [3], while for higher field strengths the enhanced many-body correlations triggered different mechanisms for the reconstruction of a stable electronic configuration, the so-called maximum density droplet, such as formation of a hole in the centre of the QD or at the edge or a spin texture [47].

A spatial deformation, i.e., a lowering of the symmetry of the artificial confinement, provides further insight as regards our understanding and control of the electronic properties of QDs. Anisotropy lifts the degeneracies of the single-particle spectrum and eliminates the magic numbers of the circular shell structure [48]. Furthermore, it might affect the total spin of a state. For example, with increasing deformation, the ground state of four electrons undergoes a transition from a spin triplet state (due to the Hund's rule for circular symmetry) to a spin singlet state. Other interesting effects arise from the possibility of tuning the degree of degeneracy in the single-particle spectrum by changing the anisotropic harmonic configuration, thereby predicting other sets of magic numbers for the shell closures. However, the reduced energetical spacing between the shells renders it more complicated to observe experimentally [48–50]. Dynamically, the anisotropy serves as a rapid path to chaos in the interacting system and, by varying it, it leads to an interplay of chaos and integrability [51, 52]. A variety of numerical approaches have been applied to investigate the lowering of the symmetry in the electronic properties of QDs. These include configuration interaction [51–57], Hartree [58], Hartree–Fock [59] and spin density functional theory [48, 60–64]. The effect of the magnetic field in the shell structure of asymmetric quantum dots has also been discussed both theoretically [65] and experimentally [50, 66]. Three-dimensional cylindrical [31, 36, 67, 68], ellipsoidal [69–71] and lens-shaped [72] QDs have also been studied.

In the present paper, a detailed investigation is performed that combines effects due to the interelectronic interaction, anisotropy and an external magnetic field in two-electron QDs with harmonic confinement by employing an 'exact' numerical diagonalization approach. In section 2, we provide the Hamiltonian of the electronic motion and discuss its general symmetries. In section 3, we introduce our basis set and present the computational approach. Section 4 contains our results. In particular, the low lying spectrum in a magnetic field and the magnetization are investigated for the full deformation regime from circularly symmetric to wirelike dots. The results are discussed also in the presence of the Zeeman splitting term. Moreover, the dynamics for a specific deformation is studied for changing magnetic field and is linked to the single-particle picture. Finally, in section 5, we provide the conclusions.

2. Hamiltonian and general symmetries

The conduction band electrons confined in a two-dimensional anisotropic harmonic quantum dot in a magnetic field $\mathbf{B} = (0, 0, B)$, within the framework of the effective mass

approximation, are described by the Hamiltonian $\mathcal{H} = \mathcal{H}_{\rm CM} + \mathcal{H}_r$ with

$$\mathcal{H}_{\rm CM} = \frac{1}{4m_{\rm e}}(\mathbf{P} + 2e\mathbf{A}(\mathbf{R}))^2 + m_{\rm e}\omega_0^2(\cos^2\phi X^2 + \sin^2\phi Y^2) \tag{1}$$

$$\mathcal{H}_r = \frac{1}{m_{\rm e}}\left(\mathbf{p} + \frac{e}{2}\mathbf{A}(\mathbf{r})\right)^2 + \frac{m_{\rm e}}{4}\omega_0^2(\cos^2\phi x^2 + \sin^2\phi y^2) + \frac{e^2}{4\pi\epsilon\epsilon_0|\mathbf{r}|}. \tag{2}$$

Due to the harmonic confinement, the centre of mass (CM) and internal motion separate. We choose for the vector potential the symmetric gauge $\mathbf{A}(\mathbf{r}) = \frac{1}{2}(\mathbf{B}\times\mathbf{r})$ and e, $m_{\rm e}$, ϵ, ω_0, ϕ are the electron charge, effective mass, dielectric constant, characteristic frequency and anisotropy parameter, respectively. Lower case and capital letters correspond to the relative and centre of mass degrees of freedom, respectively. Quantization of $\mathcal{H}_{\rm CM}$ is straightforward and direct observation of the electronic properties due to $\mathcal{H}_r$ via far infrared spectroscopy is prohibited, since radiation in the dipole approximation contains only CM degrees of freedom and decouples from $\mathcal{H}_r$ [4, 73, 74]. In the following we focus on the non-trivial relative motion $\mathcal{H}_r$. Parity ($\mathbf{r}\to-\mathbf{r}$) and spin are interrelated symmetries due to the Pauli exclusion principle and we encounter spin singlet eigenfunctions with even spatial symmetry $\Psi(\mathbf{r}) = \Psi(-\mathbf{r})$ and spin triplet eigenfunctions with odd spatial symmetry $\Psi(\mathbf{r}) = -\Psi(-\mathbf{r})$.

To simplify our Hamiltonian we apply a canonical transformation, $x = lx'$, $y = ly'$, $p_x = p_x'/l$, $p_y = p_y'/l$, thereby scaling $\mathcal{H}_r$ into a dimensionless form, via $\mathcal{H}_r = \frac{\hbar^2}{m_{\rm e}l^2}\mathcal{H}_r'$. In the following we adopt the typical values for a GaAs dot and the scaling yields the effective Bohr radius $l = a_{\rm B}^* = 9.8$ nm, the effective Hartree $Ha^* = 11.8$ meV and one effective unit (1 e.u.) of field strength corresponds to 6.925 T. The artificial (electrostatic) confinement has the characteristic frequency $\hbar\omega_0 = 4.96$ meV. This scaling yields the following expression for the dimensionless Hamiltonian of the relative motion (the primes have been dropped for simplicity):

$$\mathcal{H}_r = -\frac{\partial^2}{\partial x^2} - \frac{\partial^2}{\partial y^2} - \mathrm{i}\frac{B}{2}\left(x\frac{\partial}{\partial y} - y\frac{\partial}{\partial x}\right) + \frac{1}{4}\left(\frac{B^2}{4} + \omega_x^2\right)x^2 + \frac{1}{4}\left(\frac{B^2}{4} + \omega_y^2\right)y^2 + \frac{1}{\sqrt{x^2+y^2}}. \tag{3}$$

The two characteristic frequencies of the confinement are $\omega_x = \omega_0\cos\phi$ and $\omega_y = \omega_0\sin\phi$. For $\phi = 45°$ the dot has a circular shape. With increasing ϕ it deforms to an elliptic shape and ends up as a wirelike dot for $\phi\to 90°$ ($\omega_x\to 0$, $\omega_y\to\omega_0$).

The spin of the two electrons leads to an additional contribution to the energy, i.e., the Zeeman term,

$$E_S(B) = g^*\mu_{\rm B}BS_z \tag{4}$$

with $\mu_{\rm B}$ being the Bohr magneton and $g^* = -0.44$ the effective Landé factor for GaAs. E_S splits the threefold degeneracy of the spin triplet states while the spin singlet states remain unchanged.

3. Computational approach

To investigate the two-electron QD we solve the corresponding Schrödinger equation using a full configuration interaction (CI) approach with the anisotropic harmonic oscillator basis set

$$\Phi_{n_xn_y} = A(n_x,n_y)H_{n_x}(\sqrt{c_1}x)H_{n_y}(\sqrt{c_3}y)\exp\left(-\frac{c_1}{2}x^2 - \frac{c_3}{2}y^2 + \mathrm{i}\left(\lambda - \frac{c_2}{2}\right)xy\right) \tag{5}$$

which leads to an algebraic eigenvalue problem. In equation (5) $A(n_x, n_y)$ is the normalization constant, $c_1 = M_1\omega_1/c$, $c_3 = M_2\omega_2/c$, $c_2 = 2\mu M_1\omega_1 M_2\omega_2/c$, $c = \mu^2 M_1 M_2\omega_1\omega_2 + 1$, $\mu = -2L/(m_e\omega_0 p)$, $\lambda = [m_e\omega_0 L(2+L^2)]/[4(\cos(2\phi) - p)]$, $M_{1,2} = m_e p/(p - \cos(2\phi) \mp L^2)$, $\omega_{1,2} = (\omega_0/\sqrt{2})\sqrt{1 + L^2 \mp p}$, $L = eB/m_e\omega_0$ and $p = \sqrt{(1+L^2)^2 - \sin^2(2\phi)}$. All the units are scaled appropriately. The argument for the choice of these orbitals is the following. The single-particle anisotropic harmonic oscillator in a magnetic field, described by the Hamiltonian (3) without the Coulomb interaction term, can be transformed unitarily such that we arrive at a Hamiltonian for two independent oscillators in their individual one-dimensional harmonic potentials [75]:

$$\mathcal{H} = \frac{p_1^2}{2M_1} + \frac{p_2^2}{2M_2} + \frac{1}{2}M_1\omega_1^2 x^2 + \frac{1}{2}M_2\omega_2^2 y^2 \tag{6}$$

with eigenvalues $E_{n_1,n_2} = (n_1 + \frac{1}{2})\hbar\omega_1 + (n_2 + \frac{1}{2})\hbar\omega_2$ and eigenfunctions of the form,

$$\Psi_{n_1n_2} = N_{n_1,n_2}\exp\left(-\frac{c_1}{2}x^2 - \frac{c_3}{2}y^2 + \mathrm{i}\left(\lambda - \frac{c_2}{2}\right)xy\right) \times \sum_{k=0}^{n_1}\sum_{l=0}^{n_2} c_{kl}(n_1,n_2)H_{n_1-k}(\alpha_1 x + \beta_1 y)H_{n_2-l}(\alpha_2 x + \beta_2 y). \tag{7}$$

The exponential part in $\Psi_{n_1n_2}$ is exactly contained in our basis set (see equations (5) and (7)). The analytical expressions for the coefficients $c_{kl}(n_1, n_2)$, α_1, β_1, α_2, β_2 in equation (7) can be found in [75]. The Hermite polynomials $H_{n_1-k}(\alpha_1 x+\beta_1 y)$ and $H_{n_2-l}(\alpha_2 x+\beta_2 y)$ in equation (7) can be equally described by the Hermite polynomials of our basis set in equation (5). The corresponding relation is given by [76]

$$H_{n_1-k}(\alpha_1 x + \beta_1 y) = \frac{1}{\sqrt{2^{n_1-k}}}\sum_{i=0}^{n_1-k} H_{n_1-k-i}(\sqrt{2}\alpha_1 x)H_i(\sqrt{2}\beta_1 y).$$

Therefore, in order to describe exactly the eigenstate $\Psi_{n_1n_2}$ with our basis set, we need to superimpose Hermite polynomials of equation (5) up to maximal order $n_x = n_y = n_1 + n_2$.

The next step is evaluating the Hamiltonian matrix belonging to equation (3). For this purpose, we find firstly a Hamiltonian which can be diagonalized exactly and then subtract it from $\mathcal{H}_r$. To proceed, we write down the orbitals $\Phi_{n_xn_y} = \tilde{\Phi}_{n_xn_y}\mathcal{P}$, where $\mathcal{P} = \exp(\mathrm{i}(\lambda - \frac{c_2}{2})xy)$ is the phase and $\tilde{\Phi}_{n_xn_y}$ are the eigenfunctions of the dimensionless scaled Hamiltonian

$$\tilde{\mathcal{H}}_0 = -\frac{1}{2}\frac{\partial^2}{\partial x^2} - \frac{1}{2}\frac{\partial^2}{\partial y^2} + \frac{1}{2}c_1^2 x^2 + \frac{1}{2}c_3^2 y^2$$

with eigenvalues $\tilde{\varepsilon}_{n_xn_y} = (n_x + \frac{1}{2})\hbar c_1 + (n_y + \frac{1}{2})\hbar c_3$. To implement the phase we proceed as follows:

$$\tilde{\mathcal{H}}_0\tilde{\Phi}_{n_xn_y} = \tilde{\varepsilon}_{n_xn_y}\tilde{\Phi}_{n_xn_y} \Rightarrow \mathcal{P}\tilde{\mathcal{H}}_0\mathcal{P}^{-1}\mathcal{P}\tilde{\Phi}_{n_xn_y} = \tilde{\varepsilon}_{n_xn_y}\mathcal{P}\tilde{\Phi}_{n_xn_y} \Rightarrow \mathcal{H}_0\Phi_{n_xn_y} = \tilde{\varepsilon}_{n_xn_y}\Phi_{n_xn_y}$$

where $\mathcal{H}_0 = \mathcal{P}\tilde{\mathcal{H}}_0\mathcal{P}^{-1}$. For our QD we have to consider the Hamiltonian $\mathcal{H}_1 = 2\mathcal{H}_0$ with eigenvalues $\eta_{n_xn_y} = 2\tilde{\varepsilon}_{n_xn_y}$ where

$$\mathcal{H}_1 = -\frac{\partial^2}{\partial x^2} - \frac{\partial^2}{\partial y^2} + 2\mathrm{i}\left(\lambda - \frac{c_2}{2}\right)\left(x\frac{\partial}{\partial y} + y\frac{\partial}{\partial x}\right) + \left[\left(\lambda - \frac{c_2}{2}\right)^2 + c_1^2\right]x^2 + \left[\left(\lambda - \frac{c_2}{2}\right)^2 + c_3^2\right]y^2.$$

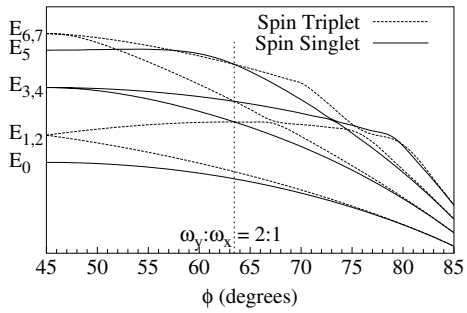

Figure 1. A schematic diagram of the energy of the ground and first seven excited states for $B = 0$ with increasing ϕ. The vertical line indicates the angle for which the system is integrable.

Therefore, the dimensionless Hamiltonian of the relative motion $\mathcal{H}_r$ can be written as

$$\begin{aligned}\mathcal{H}_r = (\mathcal{H}_r - \mathcal{H}_1) + \mathcal{H}_1 = &-\mathrm{i}\left[-\frac{B}{2} + 2\left(\lambda - \frac{c_2}{2}\right)\right] y\frac{\partial}{\partial x} - \mathrm{i}\left[\frac{B}{2} + 2\left(\lambda - \frac{c_2}{2}\right)\right] x\frac{\partial}{\partial y} \\ &+ \left[\frac{B^2}{16} + \frac{\omega_x^2}{4} - \left(\lambda - \frac{c_2}{2}\right)^2 - c_1^2\right] x^2 \\ &+ \left[\frac{B^2}{16} + \frac{\omega_y^2}{4} - \left(\lambda - \frac{c_2}{2}\right)^2 - c_3^2\right] y^2 + \frac{1}{\sqrt{x^2 + y^2}} + \mathcal{H}_1. \end{aligned} \tag{8}$$

The eigenvalues $\eta_{n_x n_y}$ will be contained in the diagonal elements of the Hamiltonian matrix. The matrix elements due to the contribution of the first four terms in equation (8) can be calculated in a straightforward analytical form. The matrix elements due to the Coulomb repulsion have to be evaluated numerically. For this purpose, we replace the Coulomb interaction by an auxiliary Gaussian integral, the so-called Singer transform, resulting in a three-dimensional integral. A combination of Gauss–Hermite exact expressions for the integrals in x and y and a Gauss–Kronrod quadrature in the auxiliary integration allow an efficient and in particular accurate evaluation of the electron–electron integral. A complete analytical evaluation of the Coulomb integral is also possible but yields a fourfold series which turns out to be numerically unstable. For further details on the treatment of the electron–electron integrals we refer the reader to [51, 52].

4. Results and discussion

4.1. No magnetic field

The starting point of our analysis is the two-electron anisotropic quantum dot without a magnetic field, which has been studied in detail in [51, 52]. Figure 1 presents the low lying spectrum of $\mathcal{H}_r(B = 0)$ as a function of the anisotropy ϕ. For $\phi = 45°$ the dot is rotationally symmetric and L_z is a constant of motion. The energy eigenstates follow (with increasing energy) the symmetries: $(m; S) = (0; 0), (\pm 1; 1), (\pm 2; 0), (0; 0), (\pm 3; 1), (\pm 1; 1), \ldots$, where m and S are the magnetic quantum number and the total spin, respectively. The introduction of the anisotropy splits the degeneracies and leads to spin singlet–triplet (ST) crossings. At $\omega_y{:}\omega_x = 2{:}1$, $\mathcal{H}_r(B = 0)$ becomes integrable due to the constant of motion:

$$\Lambda = \{L_z, p_x\} + \frac{\omega_x^2}{2} y x^2 - \frac{y}{\sqrt{x^2 + y^2}}.$$

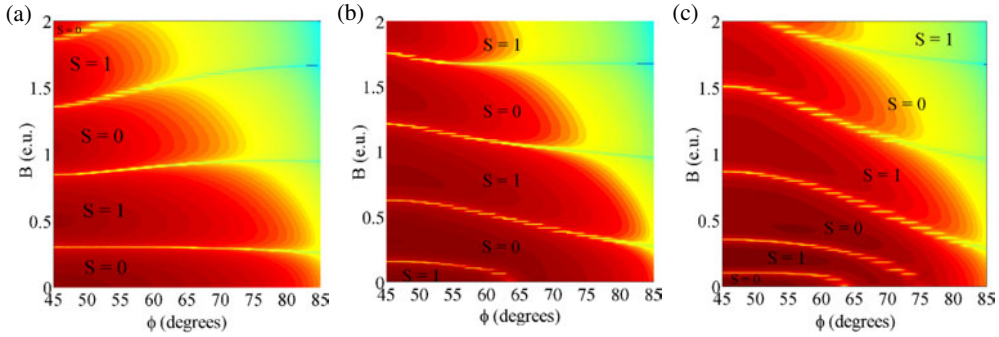

Figure 2. Domains of spin multiplicity in the (B, ϕ) plane for (a) the ground state, (b) the second excited state and (c) the fourth excited state. The brightness indicates the energy differences ΔE_0, ΔE_2 and ΔE_4, on a logarithmic scale. Dark and bright regions correspond to large and small spacings, respectively. The bright curves form the borders between the different ST symmetry domains.

Both the x-parity and the y-parity are symmetries of $\mathcal{H}_r(B = 0)$ for any ϕ. Λ commutes with the x-parity but not with the y-parity operator leading to pairwise degeneracies of ST states with identical x-parity. For $\phi \to 90°$ the eigenstates converge to energetically well-separated pairs of spin singlet and spin triplet states.

4.2. The spectrum and magnetization for $g^* = 0$ in a magnetic field

Before investigating the general situation of our interacting anisotropic QD in a magnetic field let us briefly address the effect of the magnetic field in the interacting isotropic case, which possesses particular analytical solutions [67, 77]. L_z is a constant of motion and the system is integrable. As stated in the introduction, increasing the magnetic field leads to a ground state for the system that changes its spin symmetry, i.e., the well-known ground state ST oscillations [35]. The symmetries of the ground state with increasing magnetic field are as follows: $(m; S) = (0; 0), (-1; 1), (-2; 0), (-3; 1), \ldots$. With increasing field strength, the energy spacing between two neighbouring levels $\Delta E_i = E_{i+1} - E_i$ (i determines the degree of excitation and takes even values $i = 0, 2, 4$ within our study) oscillates between zero (at the ST crossing of the states with energies E_i and E_{i+1}) and a maximum amplitude $\Delta E_{\max}$. For stronger external fields $\Delta E_{\max}$ reduces and the energy curves of the ground and first excited state have a slope that approaches the same constant value. A quantity for measuring this event is the magnetization, which, at zero temperature, is defined as $M(B) = -(\frac{\partial E_0}{\partial B})$, where E_0 is the energy of the ground state. Hence, the ST crossings will appear as steps in the magnetization curve whose size decreases for strong magnetic fields (see figure 3 for $\phi = 45°$).

Introduction of the anisotropy breaks the rotational symmetry and a large number of avoided crossings between the energy curves of states with identical symmetry occurs. For $B = 0$ the level spacing ΔE_0 will decrease with increasing deformation (see figure 1). Figure 2(a) shows the spin multiplicity $S = 0, 1$ of the ground state in the (B, ϕ) plane. For $\phi = 45°$ we observe the ST ground state oscillations, discussed in the previous paragraph. With increasing deformation we observe a robustness of the border curve $B(\phi)$ corresponding to the first ST crossing, i.e., it is approximately independent of ϕ. For higher magnetic fields the domains corresponding to different spin multiplicity widen smoothly with increasing deformation and the corresponding curves $B(\phi)$ show a significant positive slope $\frac{dB}{d\phi}$. As a

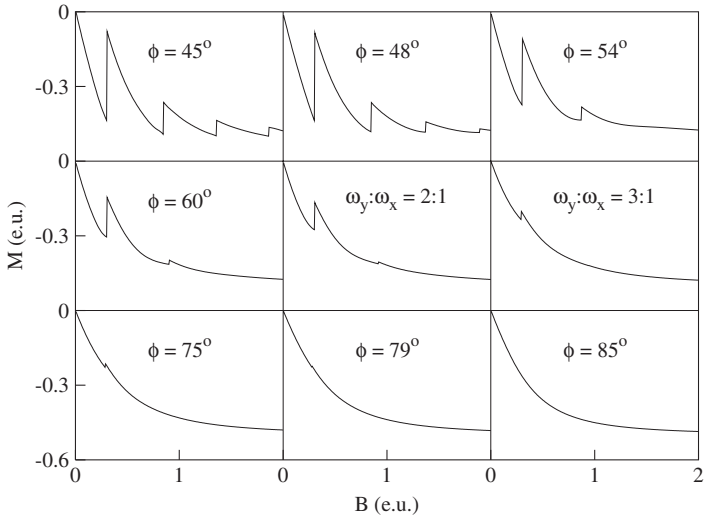

Figure 3. The magnetization $M(B)$ for $g^* = 0$. The various panels correspond to anisotropies covering the full deformation regime.

result the fifth $S = 0$ domain is suppressed for $\phi \gtrsim 54°$ in the range of the calculated magnetic field strengths.

Figure 2(b) shows the spin multiplicity domains for the second excited state (E_2) in the (B, ϕ) plane. For $B = 0$ this state is a spin triplet state and at $\omega_y{:}\omega_x = 2{:}1$ it becomes degenerate with the spin singlet state corresponding to the energy E_3 (see figure 1 and the discussion in section 4.1 for further details). For larger ϕ the state with energy E_2 is a spin singlet. The border curve corresponding to the first ST crossover for relatively weak magnetic fields stops at $\omega_y{:}\omega_x = 2{:}1$ at $B = 0$. The following border curves for stronger fields show a negative slope and the different symmetry domains slightly widen for stronger anisotropies $\omega_y{:}\omega_x > 2{:}1$.

The fourth excited state (E_4) shows an even stronger dependence of its spin multiplicity islands on B and ϕ. Figure 2(c) shows the spin symmetry domains for the fourth excited state. Initially it is a spin singlet and after $\omega_y{:}\omega_x = 2{:}1$ it becomes a spin triplet due to a ST crossing as expected. For stronger anisotropies and due to the higher number of excited states involved in the spectrum, at $\phi \approx 75°$ an 'accidental' crossing occurs and the fourth excited state restores its initial parity. With increasing magnetic fields the first boundary curve is suppressed at $\omega_y{:}\omega_x = 2{:}1$ and the second one at $\phi \approx 75°$ as a result of the above discussed behaviour. For stronger field, the corresponding spin multiplicity domains and border curves show an even stronger dependence on ϕ than the one observed for the second excited state.

A complementary quantity for studying the separate implications of the magnetic field and deformation on the ground state is the magnetization M. It has been shown that for three and four electrons M depends on both the anisotropy and the number of electrons [58]. Figure 3 shows the magnetization for various anisotropies corresponding to the full deformation regime. For $\phi = 45°$ the steps are more pronounced than for any anisotropy. With increasing ϕ the overall behaviour of $\Delta E_0(B)$ leads to a decrease of the steps in the magnetization signal, despite the fact that the ST oscillations are present according to figure 2(a). Hence, at $\phi \gtrsim 54°$ the fourth step is eliminated as predicted by figure 2(a) but also the third step is no longer visible on the scale of figure 3 for $\phi \gtrsim 54°$, the second step disappears for $\phi \gtrsim 70°$ and the first one disappears for $\phi \gtrsim 81°$ resulting in a completely smooth behaviour for $\phi = 85°$.

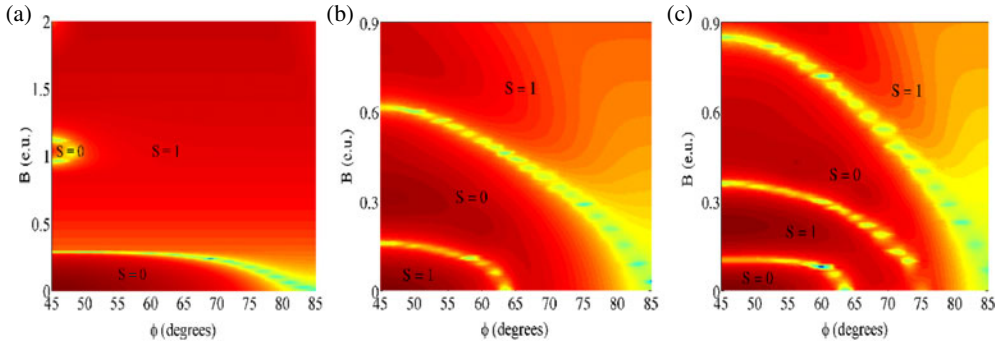

Figure 4. Domains of spin multiplicity in the (B, ϕ) plane for (a) the ground state, (b) the second excited state and (c) the fourth excited state in the presence of spin Zeeman splitting. Brightness indicates the energy differences ΔE_0, ΔE_2 and ΔE_4, on a logarithmic scale. Dark and bright regions correspond to large and small spacings, respectively. The bright curves form the borders between the different ST symmetry domains.

4.3. The spectrum and magnetization for $g^* = -0.44$

So far, in our discussion, we have neglected the contribution of the Zeeman term (given by equation (4)) in the calculation of the spectrum. The Zeeman term E_S splits the threefold degeneracy of the spin triplet states while it leaves unchanged the spin singlet states. This additional splitting in the energy of the spin triplet states reduces the amplitude $\Delta E_{\max}$ in the oscillations of the level spacing ΔE_0 and suppresses the ST oscillations in favour of the spin triplet symmetry. Figure 4(a) shows the spin multiplicity of the ground state in the presence of the Zeeman term. For $\phi = 45°$, despite the fact that the first ST oscillation survives, preserving the first $S = 0$ domain, the second spin singlet domain is clearly reduced in comparison with figure 2(a) whereas the third $S = 0$ domain in figure 2(a) vanishes completely. The introduction of a deformation results in an elimination of the second spin singlet island for angles $\phi \gtrsim 48°$. The first $S = 0$ domain is preserved up to $\phi \approx 65°$ while for stronger anisotropies E_S dominates due the reduced level spacing $\Delta E_0(B = 0)$ and the $S = 0$ domain smoothly decreases in size with further increasing deformation ϕ.

Figures 4(b) and (c) show the ST oscillations for the second (E_2) and fourth (E_4) excited state in the (B, ϕ) plane respectively. It is clear that for lower fields, where E_S is negligible due to the small effective Landé factor for GaAs, the ST oscillations as described in figures 2(b) and (c) persist with varying ϕ. For stronger external field (note that figures 4(b) and (c) cover only the weak to intermediate field regime $B \leqslant 0.9$ whereas figures 2 cover the range $B \leqslant 2.0$) the picture is rather complicated due to the competition of the existing energy scales belonging to E_S and the level spacing as well as the large number of excited states involved in the formation of the spectrum. For a better illustration of our results, we present the low lying spectrum for two anisotropies corresponding to the intermediate (ω_y:ω_x = 2:1) and the wirelike ($\phi = 81°$) regime in figure 5. In both pictures we can observe the suppression of the spin singlet states in the ground state as reproduced in figure 4(a) (note that all spin multiplet components are shown in figure 5). For higher excited states, in the intermediate anisotropic regime we observe avoided crossings and the ST oscillations are preserved for the low field regime while in the wirelike case the pairing of the states leads to a rapid suppression of the spin singlet states in this extreme limit.

In order to complete our analysis for $g^* = -0.44$ we study the behaviour of the magnetization. Figure 6 presents the magnetization for various anisotropies. For $\phi = 45°$ we

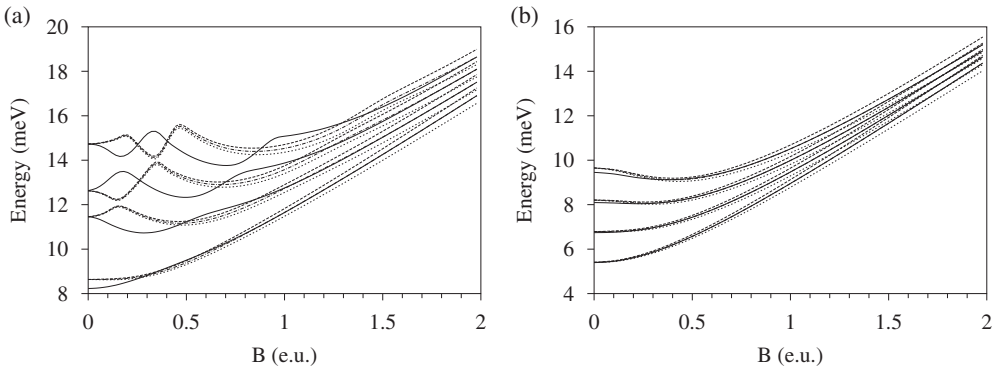

Figure 5. The low lying spectrum for (a) $\omega_y{:}\omega_x = 2{:}1$ and (b) $\phi = 81°$. Full curves correspond to spin singlet symmetry while the broken ones correspond to spin triplet symmetry with $S_z = \pm 1, 0$.

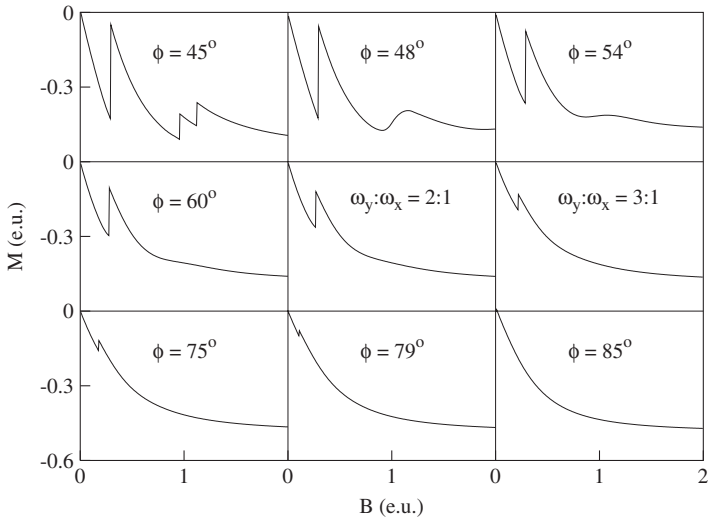

Figure 6. The magnetization $M(B)$ for $g^* = -0.44$. The various panels correspond to anisotropies covering the full deformation regime.

observe the first step remaining almost intact in the presence of E_S reflecting the robustness of the first $S = 0$ domain for the ground state energy. The next two steps are reduced in height and their location in terms of field strengths is changed significantly compared to $g^* = 0$, as expected from the discussion of figure 4(a). For $\phi \gtrsim 48°$ the second and third steps turn into a hill, due to the suppression of the spin singlet island, which gradually disappears with increasing anisotropy. The first step preserves its position up to $\phi \approx 65°$ while for stronger deformations it shifts towards lower field strengths due to the competition of E_S and $\Delta E_0(B = 0)$ in the wirelike regime. For $\phi = 85°$ the magnetization shows a completely smooth diamagnetic behaviour.

4.4. Dynamics

Before we investigate the dynamics of our interacting dot let us address some features of the single-particle system, i.e. the Hamiltonian (6) which describes the (diagonalized) anisotropic

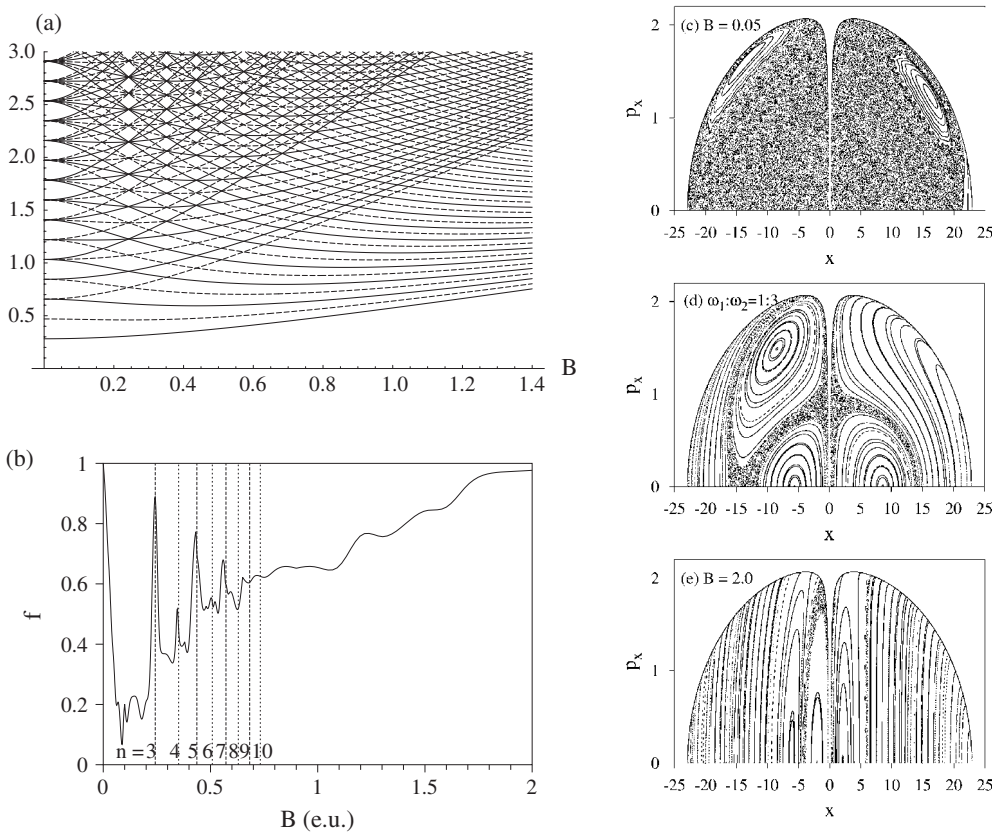

Figure 7. (a) The single-particle spectrum; full curves correspond to spin singlet states and broken curves to spin triplet states, (b) the fraction f of regular phase space as a function of the magnetic field for the interacting dot and ((c)–(e)) Poincaré surfaces of the section (x, p_x for $y = 0$ and $E = 55$ meV) for various magnetic fields (ω_y:$\omega_x = 2$:1, $\hbar\omega_0 = 4.96$ meV for all subfigures).

charged oscillator in a magnetic field. Its eigenvalues are $E_{n_1,n_2} = (n_1 + \frac{1}{2})\hbar\omega_1 + (n_2 + \frac{1}{2})\hbar\omega_2$. Figure 7(a) illustrates the single-particle spectrum at the anisotropic harmonic configuration ω_y:$\omega_x = 2$:1 with varying field strength. For $B = 0$ we observe the energy gaps due to the $[\frac{N_0}{2} + 1]$-fold degeneracy (the brackets [ ] indicate the integer part of the enclosed number) of the energy levels where $N_0 = n_1 + 2n_2 = 0, 1, 2, \ldots$. For finite field strengths the degeneracies are lifted. For rational frequency ratios ω_1:$\omega_2 = 1$:n, where $n \geqslant 3$ is integer, the energy levels become $[\frac{N_1}{n} + 1]$-fold degenerate where $N_1 = n_1 + nn_2 = 0, 1, 2, \ldots$. Hence, by varying the magnetic field we can tune the degeneracies of the single-particle spectrum as has been already noted in [78]. The values of the field strengths for which we encounter ω_1:$\omega_2 = 1$:n are given by the expression

$$B = \omega_0 \sqrt{\sin 2\phi \left(\frac{n^2 + 1}{2n} \right) - 1}.$$

Table 1 contains the values of the field strength corresponding to $n = 3$–10. With increasing n the level spacing between two neighbouring degenerate manifolds reduces. In the high field limit the energy levels corresponding to states with $n_2 = 0$ cluster to form the lowest Landau level, the energies corresponding to $n_2 = 1$ the first excited Landau level etc (see figure 7(a)

Table 1. Field strengths corresponding to the frequency ratios $\omega_1{:}\omega_2 = 1{:}n$ ($\hbar\omega_0 = 4.96$ meV, $\omega_y{:}\omega_x = 2{:}1$).

n	Magnetic field (e.u.)
3	0.242 487
4	0.351 397
5	0.436 477
6	0.508 645
7	0.572 364
8	0.63
9	0.682 993
10	0.732 295

for large B values). Another property of the single-particle degenerate manifolds is that those corresponding to odd n consist exclusively either of spin singlet or of spin triplet states whereas those corresponding to even n consist of both spin singlet and triplet states.

Let us now discuss the dynamics of the interacting system following the same path as before when studying the single-particle spectrum, i.e., starting with $\omega_y{:}\omega_x = 2{:}1$ and increasing B. The parameter characterizing the dynamics is the fraction of regular phase space defined as $f =$ (number of regular trajectories)/(total number of trajectories). The criterion for whether a trajectory is regular or chaotic is, of course, the finiteness of the Lyapunov exponent. Figure 7(b) shows f as a function of the magnetic field. For $B = 0$ the system, as discussed in section 4.1, is integrable and therefore $f = 1$. Introduction of the external field serves as a rapid path to chaos. Figure 7(c) shows a Poincaré surface of the section (PSOS) for $B = 0.05$. It can be seen that even for such a weak field, the regularity is dramatically suppressed and the phase space is dominated by chaos. Further increasing the field strength we are led to an impressive peak for f at $B = 0.242\,487$. This field strength corresponds to the frequency ratio $\omega_1{:}\omega_2 = 1{:}3$. The next major peak of $f(B)$ in figure 7(b) occurs at $\omega_1{:}\omega_2 = 1{:}4$ and consequently at $\omega_1{:}\omega_2 = 1{:}n$ for $n \geqslant 5$. We observe that the peaks of $f(B)$ corresponding to odd n are in general more pronounced than those corresponding to even n. However, the two cases lead to a similar level clustering for the quantized system. Although we cannot provide a thorough explanation for this, we remark that the states for a given cluster of levels corresponding to a frequency ratio with odd n possess the same parity (i.e., either spin singlet or spin triplet), while the states of a given cluster of levels corresponding to even n involve both parities (i.e., spin singlet and spin triplet). From this behaviour of f we conclude that interaction effects of the QD usually destroy the regularity of classical phase space, but at rational frequency ratios $\omega_1{:}\omega_2 = 1{:}n$ regularity still plays an important role and dominates the phase space (see also figure 7(d) for $\omega_1{:}\omega_2 = 1{:}3$). Of course, this behaviour is only well pronounced for not too large values of n and the overall tendency of f with increasing field strength is to increase, finally leading to a dominant regular phase space for a very strong field (see figures 7(b) and (e) for $B = 2.0$). In this limit the magnetic interaction dominates and the anisotropic confinement due to the geometry of the dot is of perturbative character, i.e., we encounter an approximate rotational symmetry and we are close to integrability. For $B = 0$ and changing ϕ the property of dominant regular classical phase space at ratios $\omega_x{:}\omega_y = 1{:}n$ is reflected in the quantum behaviour of the dot as follows. The energy level degeneracies at the ratios $\omega_x{:}\omega_y = 1{:}n$ for the non-interacting system are rather robust with respect to interaction effects in the sense that energy level clustering occurs at these ratios (for not too large n) if the interaction between the electrons is included [51, 52]. For finite magnetic field strengths the above-observed enhanced fraction of regularity in classical phase space for the ratios $\omega_1{:}\omega_2 = 1{:}n$ of the interacting

system is reflected also in the quantum spectrum, i.e., we encounter level clustering for higher excited states.

5. Conclusions

To conclude, we performed a detailed investigation of the effects of electronic interaction, anisotropy and magnetic field interaction in the electronic structure and dynamical properties of two-electron QDs with harmonic confinement. We have calculated the low lying energy spectrum of the two-electron QD in a magnetic field for the full deformation regime from circular to wirelike dots. The calculation reveals the ground state ST oscillations for $\phi = 45°$ and their weak dependence on the anisotropy. Despite this robustness of the ground state ST oscillations the magnetization is much more sensitive to the anisotropy in the sense that it smooths, i.e., it gradually looses its step-like structure, with increasing ϕ. Furthermore, we study the excited states and reveal their ST oscillations which depend not only on the magnetic field but also significantly on the anisotropy. If we include the Zeeman splitting E_S contribution to the energy, the picture for the ground state ST oscillations changes as the spin singlet states are suppressed in favour of the spin triplet ones. The competition of the energy scales of E_S and ΔE_0 destroy already for $\phi \gtrsim 48°$ the second spin singlet island, yielding a bump in the magnetization, whereas the first spin singlet domain is eliminated with increasing ϕ. For higher excited states and intermediate field strengths the ST oscillations persist as shown for example for the second and fourth excited states. Finally, we have investigated the dynamics of the interacting system for the specific deformation $\omega_y{:}\omega_x = 2{:}1$. Despite the interaction, we find a phase space that is dominated by regularity for rational ratios $\omega_1{:}\omega_2 = 1{:}n$. For stronger field strengths the Hamiltonian acquires an approximate rotational symmetry and approaches integrability.

Acknowledgments

Financial support in the framework of the IKYDA programme of the DAAD (Germany) and IKY (Greece) is gratefully acknowledged.

References

[1] Reimann S M and Manninen M 2002 *Rev. Mod. Phys.* **74** 1283
[2] Kouwenhoven L P, Austing D G and Tarucha S 2001 *Rep. Prog. Phys.* **64** 701
[3] Tarucha S, Austing D G, Honda T, van der Hage R J and Kouwenhoven L P 1996 *Phys. Rev. Lett.* **77** 3613
[4] Maksym P A and Chakraborty T 1990 *Phys. Rev. Lett.* **65** 108
[5] Merkt U, Huser J and Wagner M 1991 *Phys. Rev.* B **43** 7320
[6] Maksym P A and Chakraborty T 1992 *Phys. Rev.* B **45** 1947
[7] Maksym P A 1993 *Physica* B **184** 385
[8] Pfannkuche D, Gudmundson V and Maksym P A *Phys. Rev.* B **47** 2244
[9] Pfannkuche D, Gerhardts R R, Gudmundson V and Maksym P A 1993 *Physica* B **189** 6
[10] Hawrylak P 1993 *Phys. Rev. Lett.* **71** 3347
[11] E Yang S-R, MacDonald A H and Johnson M D 1993 *Phys. Rev. Lett.* **71** 3194
[12] Palacios J J, Martín-Moreno L, Chiappe G, Louis E and Tejedor C 1994 *Phys. Rev.* B **50** 5760
[13] Pfannkuche D and Ulloa S E 1995 *Phys. Rev. Lett.* **74** 1194
[14] Maksym P A, Hallam L D and Weis J 1995 *Physica* B **212** 213
[15] Eto M 1997 *Japan. J. Appl. Phys.* **36** 3924
[16] Wójs A and Hawrylak P 1997 *Phys. Rev.* B **56** 13227
[17] Lamouche G and Fishman G 1998 *J. Phys.: Condens. Matter* **10** 7857
[18] Xin-Qiang W and Ling-Feng M 1998 *J. Phys.: Condens. Matter* **10** 11025
[19] Eto M 1999 *Japan. J. Appl. Phys.* **38** 376

[20] Ruan W Y and Cheung H-F 1999 *J. Phys.: Condens. Matter* **11** 435
[21] Mikhailov S A and Savostianova N A 2002 *Phys. Rev.* B **66** 033307
[22] Mikhailov S A 2002 *Phys. Rev.* B **66** 153313
[23] Tavernier M B, Anisimovas E, Peeters F M, Szafran B, Adamowski J and Bednarek S 2003 *Phys. Rev.* B **68** 205305
[24] Cha M-C and E Yang S-R 2003 *Phys. Rev.* B **67** 205312
[25] Szafran B, Bednarek S and Adamowski J 2003 *Phys. Rev.* B **67** 115323
[26] Lucignano P, Jouault B and Tagliacozzo A 2004 *Phys. Rev.* B **69** 045314
[27] El-Said M 1966 *Phys. Status Solidi* b **193** 105
[28] Gonzalez A, Perez R and Fileviez P 1997 *J. Phys.: Condens. Matter* **9** 8465
[29] Anisimovas E and Matulis A 1998 *J. Phys.: Condens. Matter* **10** 601
[30] Ruan W Y, Chan K S, Ho H P and Pun E Y 2000 *J. Phys.: Condens. Matter* **12** 3911
[31] Nazmitdinov R G, Simonović N S and Rost J M *Phys. Rev.* B **65** 155307
[32] Klama S and Mishchenko E G 1998 *J. Phys.: Condens. Matter* **10** 3411
[33] García-Castelán R M G, Choe W S and Lee Y C 1998 *Phys. Rev.* B **57** 9792
[34] Gonzalez A 1997 *J. Phys.: Condens. Matter* **9** 4643
[35] Wagner M, Merkt U and Chaplik A V 1992 *Phys. Rev.* B **45** 1951
[36] Dineykhan M and Nazmitdinov R G 1999 *J. Phys.: Condens. Matter* **11** L83
[37] Ruan W Y, Liu Y Y, Baoi C G and Zhang Z Q 1995 *Phys. Rev.* B **51** 7942
[38] Maksym P A 1996 *Phys. Rev.* B **53** 10871
[39] Bao C G 1997 *Phys. Rev. Lett.* **79** 3475
[40] Maksym P A, Imamura H, Mallon G P and Aoki H 2000 *J. Phys.: Condens. Matter* **12** R299
[41] Ashoori R C, Stormer H L, Weiner J S, Pfeiffer L N, Baldwin K W and West K W 1993 *Phys. Rev. Lett.* **71** 613
[42] Su B, Goldman V J and Cunningham J E 1994 *Surf. Sci.* **305** 566
[43] Schmidt T, Tewordt M, Blick R H, Haug R J, Pfannkuche D, von Klitzing K, Förster A and Lüth H 1995 *Phys. Rev.* B **51** 5570
[44] van der Wiel W G, Oosterkamp T H, Jannsen J W, Kouwenhoven L P, Austing D G, Honda T and Tarucha S 1998 *Physica* B **256** 173
[45] Ciorga M, Wensauer A, Pioro-Ladriere M, Korkusinski M, Kyriakidis J, Sachrajda A S and Hawrylak P 2002 *Phys. Rev. Lett.* **88** 256804
[46] Kouwenhoven L P, Oosterkamp T H, Danoesastro M W S, Eto M, Austing D G, Honda T and Tarucha S 1997 *Science* **278** 1788
[47] Oosterkamp T H, Jannsen J W, Kouwenhoven L P, Austing D G, Honda T and Tarucha S 1999 *Phys. Rev. Lett.* **82** 2931
[48] Austing D G, Sasaki S, Tarucha S, Reimann S M, Koskinen M and Manninen M 1999 *Phys. Rev.* B **60** 11514
[49] Tarucha S, Austing D G, Honda T, van der Hage T and Kouwenhoven L P 1997 *Japan. J. Appl. Phys.* **36** 3917
[50] Tarucha S, Austing D G, Sasaki S, Tokura Y, van der Wiel W and Kouwenhoven L P 2000 *Appl. Phys.* A **71** 367
[51] Drouvelis P S, Schmelcher P and Diakonos F K 2003 *Europhys. Lett.* **64** 232
[52] Drouvelis P S, Schmelcher P and Diakonos F K 2004 *Phys. Rev.* B **69** 035333
[53] Maksym P A 1998 *Physica* B **249–251** 233
[54] Ezaki T, Mori N and Hamaguchi C 1997 *Phys. Rev.* B **56** 6428
[55] Ezaki T, Mori N and Hamaguchi C 1998 *Physica* B **249–251** 238
[56] Ezaki T, Mori N and Hamaguchi C 1998 *Semicond. Sci. Technol.* **13** A1
[57] Sun L-L, Ma F-C and Li S-S 2003 *J. Appl. Phys.* **94** 5844
[58] Magnúsdóttir I and Gudmundson V 2000 *Phys. Rev.* B **61** 10229
[59] Fujito M, Natori A and Yasunaga H 1996 *Phys. Rev.* B **53** 9952
[60] Hirose K and Wingree N S 1999 *Phys. Rev.* B **59** 4604
[61] Lee I-H, Rao V, Martin R M and Leburton J-P 1999 *Phys. Rev.* B **57** 9035
[62] Lee I-H, Kim Y-H and Ahn K-H 2001 *J. Phys.: Condens. Matter* **13** 1987
[63] Reimann S M, Koskinen M, Lindelof P E and Manninen M 1998 *Physica* E **2** 648
[64] Reimann S M, Koskinen M, Kolehmainen J, Manninen M, Austing D G and Tarucha S 1999 *Eur. Phys. J.* D **9** 105
[65] Madhav A V and Chakraborty T 1994 *Phys. Rev.* B **49** 8163
[66] Tokura Y, Sasaki S, Austing D G and Tarucha S 2001 *Physica* B **298** 260
[67] Dineykhan M and Nazmitdinov R G 1997 *Phys. Rev.* B **55** 13707
[68] Simonović N S and Nazmitdinov R G 2003 *Phys. Rev.* B **67** 041305(R)
[69] Cantele G, Ninno D and Iadonisi G 2000 *J. Phys.: Condens. Matter* **12** 9019

[70] Cantele G, Ninno D and Iadonisi G 2001 *Phys. Rev.* B **64** 125325
[71] Cantele G, Ninno D and Iadonisi G 2001 *Nano Lett.* **1** 121
[72] Lew Yan Voon L C and Willatzen M 2002 *J. Phys.: Condens. Matter* **14** 13667
[73] Kohn W 1961 *Phys. Rev.* **123** 1242
[74] Peeters F M 1990 *Phys. Rev.* B **42** 1486
[75] Dippel O, Schmelcher P and Cederbaum L S 1994 *Phys. Rev.* A **49** 4415
[76] Gradshteyn I S and Ryzhik I M 1980 *Table of Integrals, Series and Products* (New York: Academic)
[77] Taut M 1994 *J. Phys. A: Math. Gen.* **27** 1045
[78] Heiss W D and Nazmitdinov R G 1998 *JETP Lett.* **68** 915